

Supporting Information

**[M(OH)₂]₃(IO₃)(SeO₄)·H₂O (M = Ga, In): metal iodate-selenate
nonlinear optical materials with hexagonal tungsten oxide-type
topology**

Qian-Qian Chen,^{a,b} Chun-Li Hu,^a Bing-Xuan Li^a and Jiang-Gao Mao^{*a,b}

a. State Key Laboratory of Structural Chemistry, Fujian Institute of Research on the Structure of Matter,
Chinese Academy of Sciences, Fuzhou, 350002, P. R. China

b. University of Chinese Academy of Sciences, Beijing 100039, P. R. China

Email: mjjg@fjirsm.ac.cn

Table of Contents

Section	Title	Page
Table S1	Selected bond lengths (\AA) and the calculated total BVS values for $[\text{M}(\text{OH})_2]_3(\text{IO}_3)(\text{SeO}_4) \cdot \text{H}_2\text{O}$ ($\text{M} = \text{Ga 1, In 2}$).	S3
Table S2	Atomic coordinates ($\times 10^4$) and equivalent isotropic displacement parameters ($\text{\AA}^2 \times 10^3$) for $[\text{M}(\text{OH})_2]_3(\text{IO}_3)(\text{SeO}_4) \cdot \text{H}_2\text{O}$ ($\text{M} = \text{Ga 1, In 2}$).	S4
Table S3	The assignments of the infrared absorption peaks for $[\text{M}(\text{OH})_2]_3(\text{IO}_3)(\text{SeO}_4) \cdot \text{H}_2\text{O}$ ($\text{M} = \text{Ga, In}$).	S5
Table S4	Calculated dipole moments for GaO_6 , IO_3 , and SeO_4 , as well as net dipole moment for a unit cell in $[\text{Ga}(\text{OH})_2]_3(\text{IO}_3)(\text{SeO}_4) \cdot \text{H}_2\text{O}$.	S5
Figure S1	Simulated and experimental powder X-ray diffraction patterns of $[\text{M}(\text{OH})_2]_3(\text{IO}_3)(\text{SeO}_4) \cdot \text{H}_2\text{O}$ ($\text{M} = \text{Ga (a), In (b)}$).	S6
Figure S2	SEM images and their elemental distribution maps of $[\text{M}(\text{OH})_2]_3(\text{IO}_3)(\text{SeO}_4) \cdot \text{H}_2\text{O}$ ($\text{M} = \text{Ga (a), In (b)}$).	S6
Figure S3	The coordination geometries around the Ga^{3+} , I^{5+} and Se^{6+} ions in $[\text{Ga}(\text{OH})_2]_3(\text{IO}_3)(\text{SeO}_4) \cdot \text{H}_2\text{O}$.	S7
Figure S4	TGA and DTA curves of $[\text{M}(\text{OH})_2]_3(\text{IO}_3)(\text{SeO}_4) \cdot \text{H}_2\text{O}$ ($\text{M} = \text{Ga (a), In (b)}$) under the N_2 atmosphere.	S7
Figure S5	The powder X-ray diffraction patterns of the residuals of $[\text{M}(\text{OH})_2]_3(\text{IO}_3)(\text{SeO}_4) \cdot \text{H}_2\text{O}$ ($\text{M} = \text{Ga (a), In (b)}$) after decomposition at 1000 °C.	S8
Figure S6	IR spectra for $[\text{M}(\text{OH})_2]_3(\text{IO}_3)(\text{SeO}_4) \cdot \text{H}_2\text{O}$ ($\text{M} = \text{Ga (a), In (b)}$).	S8
Figure S7	UV-vis-IR spectra of $[\text{M}(\text{OH})_2]_3(\text{IO}_3)(\text{SeO}_4) \cdot \text{H}_2\text{O}$ ($\text{M} = \text{Ga (a), In (b)}$).	S9
Figure S8	The calculated band structure of $[\text{M}(\text{OH})_2]_3(\text{IO}_3)(\text{SeO}_4) \cdot \text{H}_2\text{O}$ ($\text{M} = \text{Ga (a), In (b)}$).	S9
Figure S9	The partial and total density of states for $[\text{M}(\text{OH})_2]_3(\text{IO}_3)(\text{SeO}_4) \cdot \text{H}_2\text{O}$ ($\text{M} = \text{Ga (a), In (b)}$).	S10
Figure S10	The calculated refractive indices for $[\text{M}(\text{OH})_2]_3(\text{IO}_3)(\text{SeO}_4) \cdot \text{H}_2\text{O}$ ($\text{M} = \text{Ga (a), In (b)}$).	S10

Table S1. Selected bond lengths (\AA) and the calculated total BVS values for $[\text{M}(\text{OH})_2]_3(\text{IO}_3)(\text{SeO}_4) \cdot \text{H}_2\text{O}$ ($\text{M} = \text{Ga } \mathbf{1}, \text{In } \mathbf{2}$).

1		2	
Ga(1)-O(1)	1.944(2)	In(1)-O(1)	2.121(3)
Ga(1)-O(1)#1	1.944(2)	In(1)-O(1)#1	2.121(3)
Ga(1)-O(2)	1.922(2)	In(1)-O(2)	2.094(3)
Ga(1)-O(2)#4	1.922(2)	In(1)-O(2)#4	2.094(3)
Ga(1)-O(3)	2.000(7)	In(1)-O(3)	2.162(8)
Ga(1)-O(4)	2.067(7)	In(1)-O(4)	2.205(8)
BVS (Ga)	3.20	BVS (In)	3.23
I(1)-O(3)	1.807(6)	I(1)-O(3)	1.797(8)
I(1)-O(3)#1	1.807(6)	I(1)-O(3)#1	1.797(8)
I(1)-O(3)#2	1.807(6)	I(1)-O(3)#2	1.797(8)
BVS (I)	5.10	BVS (I)	5.24
Se(1)-O(4)	1.646(7)	Se(1)-O(4)	1.635(9)
Se(1)-O(4)#3	1.646(7)	Se(1)-O(4)#3	1.635(9)
Se(1)-O(4)#4	1.646(7)	Se(1)-O(4)#4	1.635(9)
Se(1)-O(5)	1.616(11)	Se(1)-O(5)	1.606(15)
BVS (Se)	6.00	BVS (Se)	6.17
O(1)-H(1)	0.7920	O(1)-H(1)	0.8353
O(2)-H(2)	0.8196	O(2)-H(2)	0.8565

Symmetry transformations used to generate equivalent atoms: #1 -x+y, -x, z; #2 -y, x-y, z; #3 -x+y, -x+1, z; #4 -y+1, x-y+1, z.

Table S2. Atomic coordinates ($\times 10^4$) and equivalent isotropic displacement parameters ($\text{\AA}^2 \times 10^3$) for $[\text{M(OH)}_2]_3(\text{IO}_3)(\text{SeO}_4) \cdot \text{H}_2\text{O}$ (M = Ga **1**, In **2**).

1				
Atom	x	y	z	U(eq)
Ga(1)	1673.0(9)	3346.0(17)	5086.1(10)	8.1(2)
I(1)	0	0	2785.4(8)	9.6(2)
Se(1)	3333.33	6666.67	7214.3(11)	8.0(3)
O(1)	-1245(5)	1245(5)	5490(5)	10.8(12)
O(2)	757(10)	5379(5)	4779(6)	11.5(13)
O(3)	1283(5)	2566(10)	3476(6)	13.3(13)
O(4)	2097(5)	4194(10)	6744(6)	12.6(13)
O(5)	3333.33	6666.67	8556(9)	15(3)
O(1W)	-3333.33	3333.33	6861(15)	47(5)
2				
Atom	x	y	z	U(eq)
In(1)	1675.9(6)	3351.7(12)	5118.0(9)	10.33(19)
I(1)	0	0	2758.4(9)	14.9(3)
Se(1)	3333.33	6666.67	7299.9(13)	12.3(4)
O(1)	-1243(6)	1243(6)	5635(6)	13.7(17)
O(2)	714(12)	5357(6)	4711(6)	17.7(18)
O(3)	1189(6)	2379(12)	3431(7)	21.1(19)
O(4)	2194(6)	4388(13)	6831(6)	22(2)
O(5)	3333.33	6666.67	8615(12)	20(4)
O(1W)	-3333.33	3333.33	6940(20)	89(10)

Table S3. The assignments of the infrared absorption peaks for $[M(OH)_2]_3(SeO_4) \cdot H_2O$ ($M = Ga, In$).

IR peak (cm^{-1})	Assignment
3700-3200	O-H stretching bands
1637	H-O-H bending mode
1130-950	ν_3 asymmetric stretching of Se-O
950-823	ν_3 asymmetric stretching of I-O
823-670	ν_1 symmetric stretching of I-O
630-400	ν_4 asymmetric bending of Se-O and ν_2 symmetric bending of I-O

Table S4. Calculated dipole moments for GaO_6 , IO_3 , and SeO_4 , as well as net dipole moment for a unit cell in $[Ga(OH)_2]_3(SeO_4) \cdot H_2O$.

$[Ga(OH)_2]_3(SeO_4) \cdot H_2O$ ($Z = 2$)				
Polar unit	Dipole moment (D = Debyes)			
	total magnitude	x-component	y-component	z-component
$Ga(1)O_6$	0.827	$(\pm 0.004) \times 3$	$(\pm 0.079) \times 3$	$(0.823) \times 6$
$I(1)O_3$	13.891	0×2	$\pm 8.824 \times 10^{-6}$	13.891×2
$Se(1)O_4$	0.162	0×2	$\pm 8.994 \times 10^{-5}$	$(-0.162) \times 2$
Net dipole moment (a unit cell)	32.396	0	0	32.396

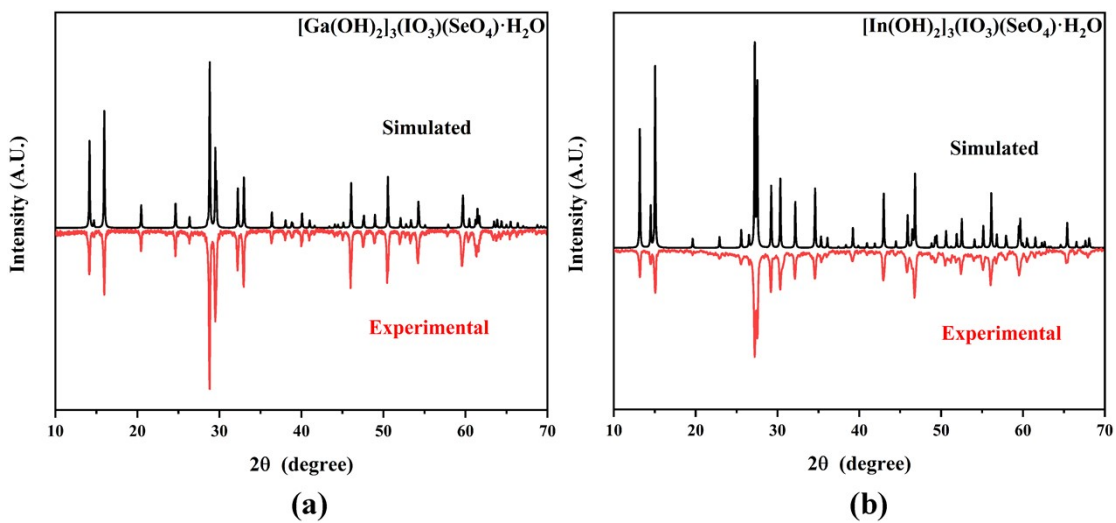


Figure S1. Simulated and experimental powder X-ray diffraction patterns of $[M(OH)_2]_3(IO_3)(SeO_4)\cdot H_2O$ ($M = Ga$ (a), In (b)).

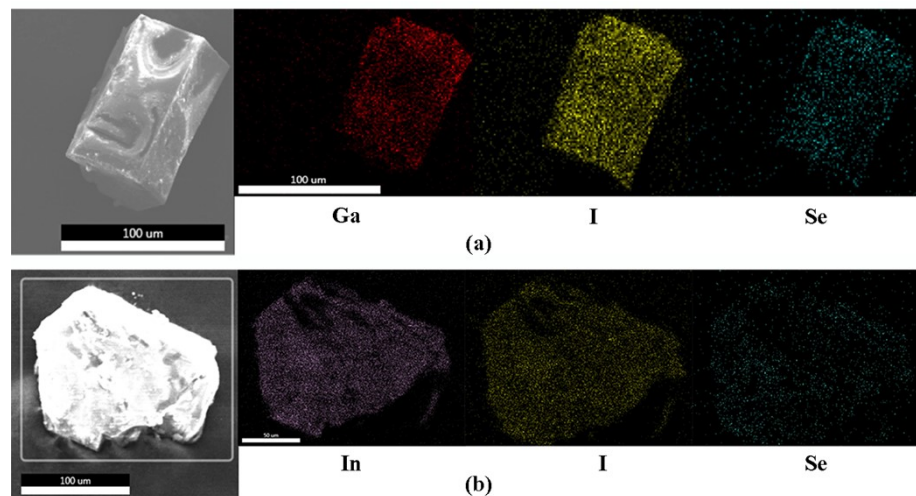


Figure S2. SEM images and their elemental distribution maps of $[M(OH)_2]_3(IO_3)(SeO_4)\cdot H_2O$ ($M = Ga$ (a), In (b)).

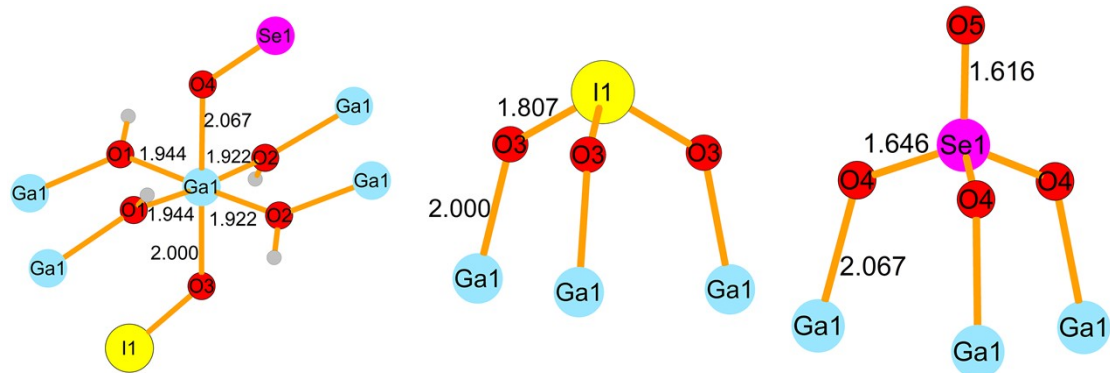


Figure S3. The coordination geometries around the Ga^{3+} , I^{5+} and Se^{6+} ions in $[\text{Ga}(\text{OH})_2]_3(\text{IO}_3)(\text{SeO}_4)\cdot\text{H}_2\text{O}$.

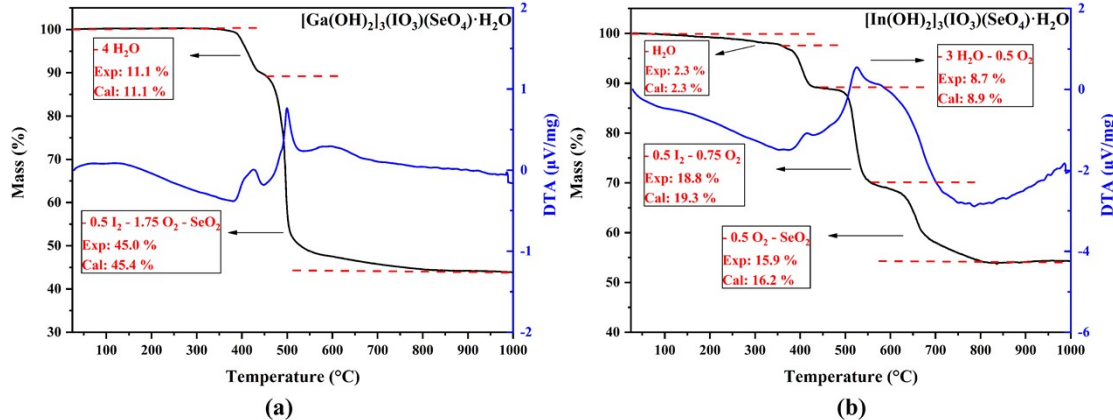


Figure S4. TGA and DTA curves of $[\text{M}(\text{OH})_2]_3(\text{IO}_3)(\text{SeO}_4)\cdot\text{H}_2\text{O}$ ($\text{M} = \text{Ga}$ (a), In (b)) under the N_2 atmosphere.

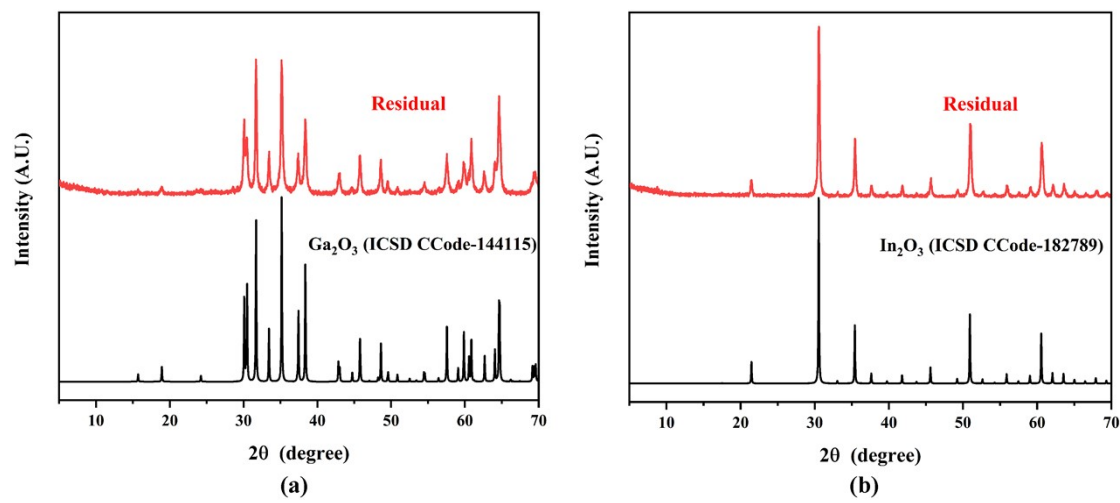


Figure S5. The powder X-ray diffraction patterns of the residuals of $[\text{M}(\text{OH})_2]_3(\text{IO}_3)(\text{SeO}_4) \cdot \text{H}_2\text{O}$ ($\text{M} = \text{Ga}$ (a), In (b)) after decomposition at 1000°C .

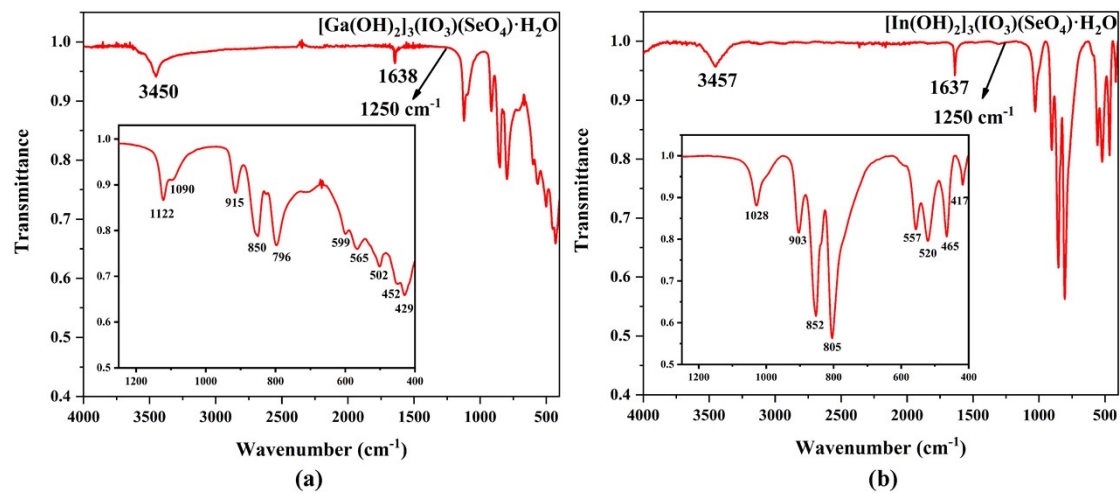


Figure S6. IR spectra for $[\text{M}(\text{OH})_2]_3(\text{IO}_3)(\text{SeO}_4) \cdot \text{H}_2\text{O}$ ($\text{M} = \text{Ga}$ (a), In (b)).

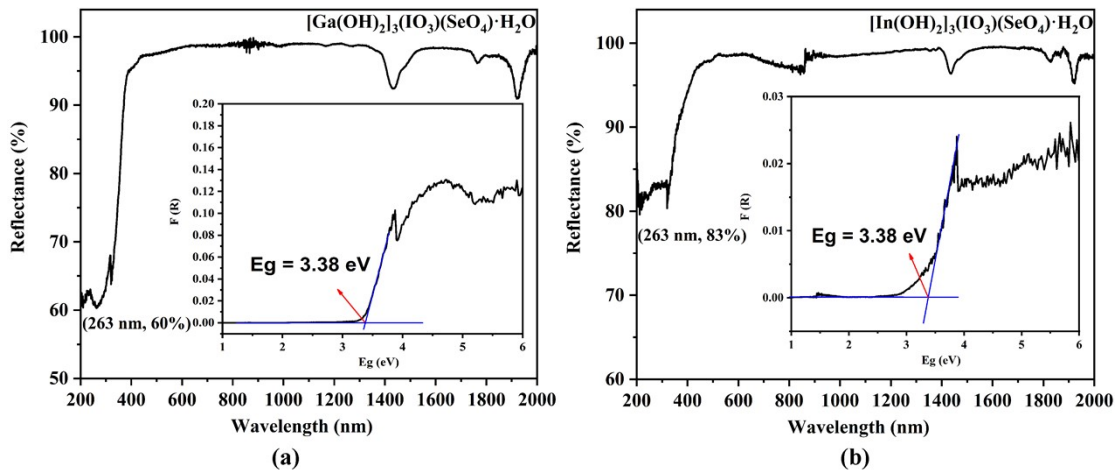


Figure S7. UV-vis-IR spectra of $[M(OH)_2]_3(PO_4)(SeO_4) \cdot H_2O$ ($M = Ga$ (a), In (b)).

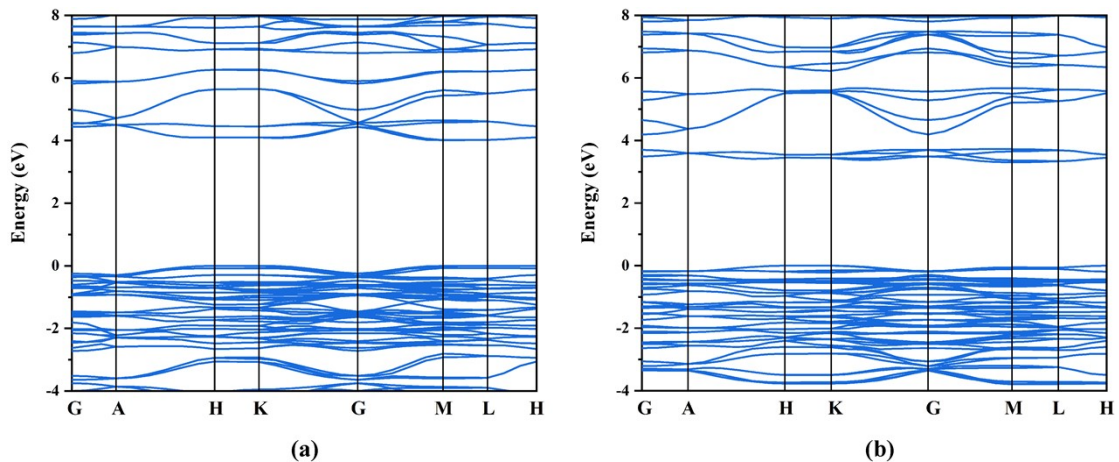


Figure S8. The calculated band structure of $[M(OH)_2]_3(PO_4)(SeO_4) \cdot H_2O$ ($M = Ga$ (a), In (b)).

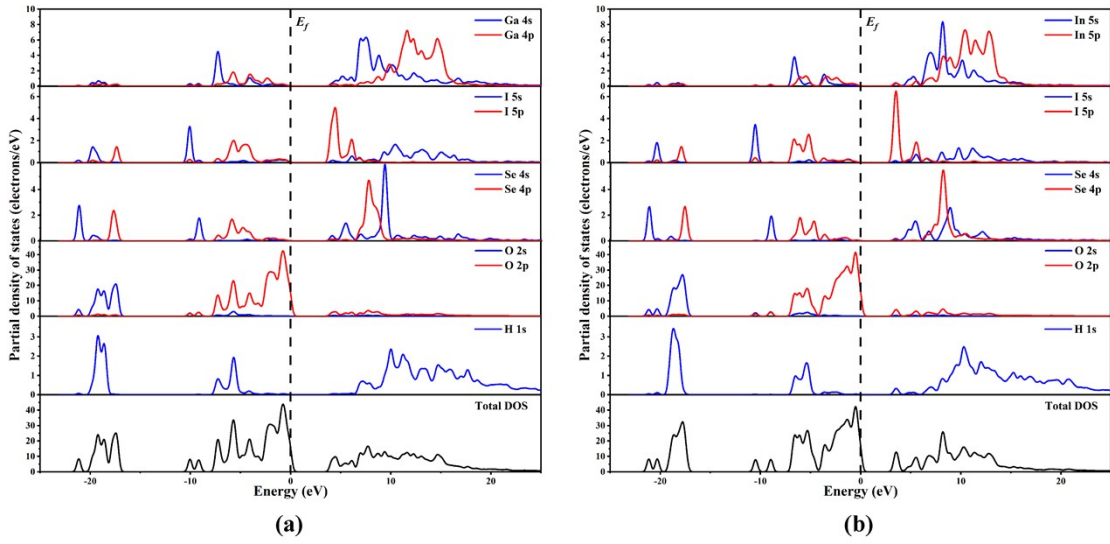


Figure S9. The partial and total density of states for $[M(OH)_2]_3(SeO_4)\cdot H_2O$ ($M = Ga$ (a), In (b)).

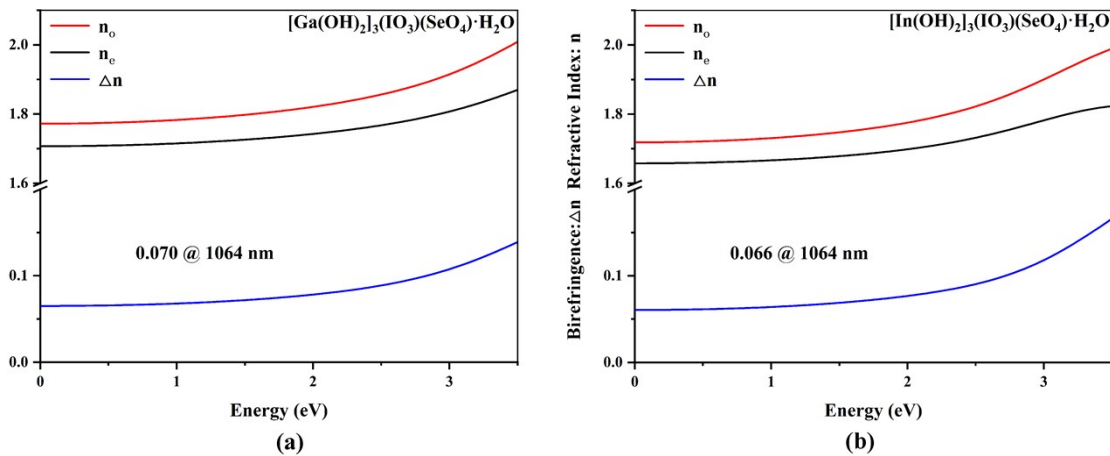


Figure S10. The calculated refractive indices for $[M(OH)_2]_3(SeO_4)\cdot H_2O$ ($M = Ga$ (a), In (b)).